Development/Plasticity/Repair

Activity Deprivation Modulates the Shank3/Homer1/mGluR5 Signaling Pathway to Enable Synaptic Upscaling

Andrea A. Guerrero and Gina G. Turrigiano
Department of Biology, Brandeis University, Waltham, Massachusetts 02453

Shank3 is an autism spectrum disorder-associated postsynaptic scaffold protein that links glutamate receptors to trafficking and signaling networks within the postsynaptic density. Shank3 is required for synaptic scaling, a form of homeostatic plasticity that bidirectionally modulates postsynaptic strength to stabilize neuronal activity. Shank3 undergoes activity-dependent phosphorylation/dephosphorylation at S1586/S1615, and dephosphorylation at these sites is critical for enabling synaptic upscaling. Here, we probe the molecular machinery downstream of Shank3 dephosphorylation that allows for synaptic upscaling in cultured rat neurons of either sex. We first show that a phosphomimetic mutant of Shank3 has reduced binding ability and interaction with long-form Homer1, a postsynaptic protein also crucial for scaling and a known binding partner of Shank3. Since metabotropic glutamate receptor 5 (mGluR5) has been shown to associate with Shank3 through long-form Homer1, we manipulated mGluR1 and mGluR5 signaling with either noncompetitive or competitive inhibitors and found that only competitive inhibition (which targets agonist-dependent signaling) impairs synaptic upscaling. Furthermore, we found that mGluR5 activation rescues synaptic upscaling in the presence of phosphomimetic Shank3 and thus is downstream of Shank3 phosphorylation. Finally, we identify signaling pathways downstream of Group I mGluRs that are necessary for upscaling. Altogether, these data show that activity-dependent dephosphorylation of Shank3 remodels the Shank3/Homer1/mGluR signaling pathway to favor agonist-dependent mGluR signaling, which is necessary to enable synaptic upscaling. More broadly, because downscaling is thought to require agonist-independent mGluR5 signaling, these findings demonstrate that synaptic up- and downscaling rely on distinct functional configurations of the same signaling elements.

Key words: homeostatic plasticity; mGluR; Shank3; synaptic plasticity; synaptic scaling

Significance Statement

Synaptic scaling is a bidirectional, homeostatic form of synaptic plasticity that allows neural circuits to maintain stable function in the face of experience-dependent or developmental perturbations. Synaptic scaling up requires dephosphorylation of the autism spectrum disorder-associated synaptic scaffold protein Shank3, but how this dephosphorylation event enables scaling up was unknown. Here we show that dephosphorylation of Shank3 rearranges interactions between synaptic proteins to drive agonist-dependent signaling through metabotropic glutamate receptors (mGluRs) and that this signaling is necessary for scaling up. These findings show that altered mGluR signaling is downstream of Shank3 during homeostatic plasticity and raise the possibility that some human Shankopathies impair signaling through this important signaling pathway.

Introduction

Synaptic scaling is a form of homeostatic plasticity that bidirectionally adjusts synaptic weights in response to prolonged changes in firing, to stabilize the activity of individual neurons and networks (Turrigiano et al., 1998; Turrigiano and Nelson, 2004; Turrigiano, 2008). A large body of work has established that synaptic scaling is expressed through changes in the postsynaptic accumulation of AMPA-type glutamate receptors (AMPAR; O'Brien et al., 1998; Gainey et al., 2009, 2015; Goold and Nicoll, 2010; Louros et al., 2018) and is accompanied by a complex remodeling of postsynaptic scaffolds (Hu et al., 2010; Sun and Turrigiano, 2011; Steinmetz et al., 2016; Venkatesan et al., 2020), but the pathways that link changes in activity to changes in synaptic AMPAR accumulation are incompletely

Received April 24, 2025; revised Sept. 16, 2025; accepted Sept. 25, 2025.

Author contributions: A.A.G. and G.G.T. designed research; A.A.G. performed research; A.A.G. analyzed data; A.A.G. and G.G.T. wrote the paper.

This work was supported by a Howard Hughes Medical Institute Gilliam Fellowship (A.A.G.) and NIH R35NS111562 (G.G.T.). We thank the Brandeis Light Microscopy Core Facility RRID:SCR_025892 for the equipment (Zeiss LSM880 and LSM880 Fast AiryScan confocal microscopes) and technical assistance. We thank Chi-Hong Wu for the invaluable mentorship, Lauren Tereshko for the Metamorph colocalization analysis scripts, and Lirong Wang for her help in generating and maintaining neuronal cultures.

The authors declare no competing financial interests.

Correspondence should be addressed to Gina G. Turrigiano at turrigiano@brandeis.edu.

This paper contains supplemental material available at: https://doi.org/10.1523/JNEUROSCI.0807-25.2025

https://doi.org/10.1523/JNEUROSCI.0807-25.2025

Copyright © 2025 the authors

understood. We recently showed that activity blockade reduces Shank3 phosphorylation at two key sites (S1586 and S1615), and this dephosphorylation is necessary for the expression of synaptic scaling up (Wu et al., 2022). Here, we focus on identifying the molecular pathways downstream of Shank3 dephosphorylation that enable synapses to undergo upscaling. We find that the phosphorylation state of Shank3 regulates binding to long-form Homer1, an interaction partner that links Shank3 to metabotropic glutamate receptors (mGluRs; Tu et al., 1999; Hayashi et al., 2009) and that agonist-dependent mGluR5 signaling is an essential downstream mediator of scaling up.

Shank3 is a multidomain scaffolding protein found abundantly at the postsynaptic density (Naisbitt et al., 1999) that interacts with several scaffold and signaling proteins known to be crucial for synaptic scaling (Grabrucker et al., 2011; Jiang and Ehlers, 2013). Synaptic upscaling depends on the dephosphorylation of two Serine sites (rat S1586/S1615) within Shank3, while synaptic downscaling requires phosphorylation of these same sites (Wu et al., 2022). One notable Shank3 interaction partner is Homer1, which has short and long isoforms—short-form Homer1a and long-form Homer1b/c. While long-form Homer1 is able to cross-link various proteins including Shanks and mGluRs, Homer1a interrupts this binding and promotes constitutive agonist-independent mGluR activity (Brakeman et al., 1997; Tu et al., 1999; Ango et al., 2001). Enhanced network activity leads to an increase in Homer1a that then shifts the balance of long-form to short-form Homer1 (Hu et al., 2010; Diering et al., 2017). This results in increased Homer1a–mGluR5 interactions (Lautz et al., 2018; Stillman et al., 2022) that lead to mGluR agonist-independent activity, thus enabling synaptic downscaling (Hu et al., 2010; Diering et al., 2017). In contrast, synaptic upscaling results in increased proteomic network associations between Shank3 and long-form Homer1 and between long-form Homer1 and mGluR5 (Heavner et al., 2021). Therefore, we hypothesized that Shank3 dephosphorylation facilitates synaptic upscaling by modulating its interaction with long-form Homer1, thus altering signaling through Group I mGluRs.

To test this hypothesis, we use quantitative immunohistochemical, biochemical, and pharmacological approaches to assess the role of long-form Homer1 and Group I mGluR signaling in synaptic scaling up. We found that scaling up protocols produced correlated increases in pre- and postsynaptic proteins and enhanced colocalization between endogenous Shank3 and long-form Homer1. This enhanced colocalization was prevented by overexpressing a phosphomimetic form of Shank3 that has reduced binding to long-form Homer1, suggesting that dephosphorylation during activity blockade is necessary for this process. We then used pharmacology to show that—in contrast to downscaling—upscaling is blocked by competitive antagonists of Group 1 mGluRs, suggesting that agonist-dependent mGluR signaling is the critical factor. Furthermore, enhancing mGluR5 signaling with a positive allosteric modulator was able to rescue synaptic upscaling in neurons overexpressing phosphomimetic Shank3, indicating that this signaling is downstream of Shank3 phosphorylation. Finally, we demonstrated that phospholipase C (PLC) and protein kinase C (PKC), downstream effectors of the canonical Group I mGluR pathway, are required for synaptic scaling up. Taken together, these data show that activity-dependent dephosphorylation of Shank3 remodels the Shank3/Homer1/mGluR signaling pathway to favor agonist-dependent mGluR signaling, and this is necessary for the induction of synaptic scaling up.

Materials and Methods

Neuronal cultures, transfection, and drug treatments. Primary neuronal cultures were prepared from the visual cortex of Long–Evans rat pups [Postnatal Days (P)1–3] of either sex from timed-pregnant dams from Charles River Laboratories. Neurons were dissociated from the primary visual cortex and plated onto glass-bottomed dishes preseeded with glial feeders, following previously described methods (Tatavarty et al., 2020; Wu et al., 2022). All experiments were performed after 7–10 d in vitro (DIV). During this period, neurons were sparsely transfected with the following constructs using Lipofectamine 2000 (Thermo Fisher Scientific). To express Shank3 phospho-mutants exogenously, GFP-tagged Shank3 constructs (2,500 ng per dish) were transfected. For better visualization of neurons during imaging, an empty GFP vector was cotransfected in both conditions. In imaging experiments measuring endogenous Shank3 and Homer1b/c, an empty GFP vector (500 ng per dish) was transfected to delineate the neurons.

For each pharmacology experiment, sister cultures were treated with vehicle as a control. Neurons aged 7–8 DIV were treated with 4 μM tetrodotoxin (TTX; Alomone Labs T-550) to induce synaptic scaling up in vitro (Turrigiano et al., 1998). The drug/vehicle was added to the cultures at the same time as TTX for a total of 24 h before fixation, except for cyclopiazonic acid (CPA) + TTX in which neurons were treated with CPA (30 μM, Tocris Bioscience 1235) for 6 h before TTX addition. For Group I mGluR inhibition experiments, MTEP + BAY condition was treated with MTEP hydrochloride (1 μM; Tocris Bioscience 2921) and BAY 36-720 (10 μM, Tocris Bioscience 2501). For probing the canonical downstream pathway of Group I mGluRs, U73122 (5 μM, Tocris Bioscience 1268), CPA (30 μM, Tocris Bioscience 1235), and GO6983 (5 μM, Tocris Bioscience 2285) were used.

For DHPG experiments, the DHPG-only condition was treated for 10 min with (*R*,*S*)-DHPG (10 μM, Tocris Bioscience 0342). The MTEP + BAY + DHPG condition was treated for a total of 1 h with MTEP hydrochloride (10 μM, Tocris Bioscience 2921) and BAY 36-720 (10 μM, Tocris Bioscience 2501) with DHPG (10 μM, Tocris Bioscience 0342) added during the last 15 min before fixation. The S4CPG + DPHG condition was treated for a total of 1 h with S4CPG (10 μM, Tocris Bioscience; 100 μM, Tocris Bioscience 0323) with DHPG (10 μM, Tocris Bioscience 0342) added during the last 15 min before fixation.

In all imaging experiments, we analyzed only excitatory pyramidal neurons, identified by their stereotypical morphology (Pratt et al., 2003). All experiments were replicated a minimum of three times from independent dissociations, with the exception of the DHPG dataset and the MTEP + BAY ± TTX data which are each from two dissociations.

Expression constructs. The short hairpin insensitive wild-type (WT) Shank3 (PDEST53) construct with an N-terminal GFP tag and the Shank3 short hairpin (PVLTHM) construct were obtained from Chiara Verpelli (Verpelli et al., 2011). Constructs expressing GFP-tagged Shank3 phospho-mutants under the control of a single CMV promoter were generated using the Gibson Assembly kit (NEB) with the WT Shank3 as the template (Wu et al., 2022). The same process was utilized to generate the GFP-tagged Shank3 P1311L point mutant and HA-tagged Homer1c, but the latter was derived from Addgene construct 54912 as a template. All constructs were verified by DNA sequencing.

HEK cell cultures and transfection. HEK 293T cells (CRL-3216, ATCC) were plated from frozen stocks onto 10 cm plates and grown in media consisting of 84% DMEM, 10% FBS, 5% Pen–Strep, and 1% L-glutamine. The HEK cells were passaged three times before plating onto six-well plates. Transfection with Lipofectamine 2000 was performed when ∼85% confluence was reached. HEK cells were cotransfected with GFP empty vector (500 ng per well) or a GFP-tagged Shank3 construct (2,450 ng per well) and WT HA-tagged Homer1c construct (1,450 ng per well).

Co-immunoprecipitation. At 24 h post-transfection, the HEK cells were washed three times with PBS (Invitrogen) and lysed with RIPA buffer containing 150 mM NaCl, 50 mM Tris–HCl, 1 mM EDTA, 1% Triton X-100, 0.1% SDS, 0.5% sodium deoxycholate, one tablet of protease inhibitor cocktail (Roche), and one tablet of PhosSTOP phosphatase

inhibitor cocktail (Roche). After sonication and centrifugation, lysates were incubated either with goat anti-rabbit GFP (A-11122) overnight followed by a 2 h incubation with Protein G Dynabeads (Thermo Fisher Scientific 1003D) or GFP-trap agarose beads or GFP-trap magnetic particles (Chromtek gtma-20, M-270) for 2 h at 4°C. The beads/particles were washed with RIPA buffer three times before eluting in 30 µl of 1× LD Buffer (Invitrogen LC2570) at 95°C for 10 min. Lysates were run on 7% Tris-Acetate gels (Invitrogen EA0358) and then transferred overnight at 4°C. Blots were blocked using Intercept PBS Blocking buffer (LICORbio) for 1 h at room temperature and then incubated with guinea pig Shank3 (Synaptic Systems 162 304) and Anti-HA-Biotin (Roche 12158167001) or goat anti-rabbit GFP (A-11122) and mouse Homer1 (Synaptic Systems 160 011) antibodies. The next day, blots were washed three times with PBS-T and incubated for 1 h with guinea pig 680RD and streptavidin 800CW or rabbit 680RD and mouse 800CW IR dye secondary antibodies (Jackson Laboratory). Western blot images were taken using BioRad imager and quantified using ImageJ (NIH).

Immunocytochemistry. Forty-eight hours post-transfection, neurons were fixed with 4% paraformaldehyde for 15 min and processed for immunocytochemistry using an established protocol (Tatavarty et al., 2020; Wu et al., 2022). Transfected neurons were identified by fluorescent protein expression. To determine the synaptic localization of endogenous or exogenously expressed Shank3, cells were permeabilized with blocking buffer (0.1% Triton X-100/5% goat serum in PBS) at room temperature for 30 min. They were then incubated overnight at 4°C in dilution buffer (5% goat serum in PBS) containing the following primary antibodies: chicken anti-GFP (1:1,000, Aves Labs GFP 10-20), rabbit anti-Shank3 (1:50, Cell Signaling #64555), and guinea pig Homer1b/c (1:500, Synaptic Systems 160 025). To visualize the surface GluA2, the protocol was modified. Prior to permeabilization, cells were first incubated for 90 min at room temperature with mouse anti-GluA2 (1:1,000, gift from Eric Gouaux, Vollum Institute, Oregon Health and Science University) diluted in blocking buffer without Triton X-100. Then, cells were permeabilized and incubated overnight at 4°C in dilution buffer (5% goat serum in PBS) with chicken anti-GFP (1:1,000, Aves Labs GFP 10-20) and anti-VGluT1 (1:1000, Synaptic Systems 135 304). For DHPG experiments, guinea pig anti-MAP2 (1:1,000, Synaptic Systems 188 004) was used to visualize the soma and projections of neurons. In addition, mouse anti-pERK1/2 (1:250, Millipore Sigma M9692) and rabbit anti-phospho-mTOR (1:100, Cell Signaling Technology 2971) were used to label phorphorylated ERK1/2 and phosphorylated mTOR, respectively.

The next day, neurons were washed three times with PBS and incubated for 1 h at room temperature with dilution buffer containing the following secondary antibodies (1:400, Thermo Fisher Scientific): goat anti-chicken Alexa Fluor 488, goat anti-mouse Alexa Fluor 555, goat anti-guinea pig Alexa Fluor 647 for sGluA2 and VGlut1 staining. For Shank3 and Homer1b/c staining, goat anti-chicken Alexa Fluor 488, goat anti-rabbit Alexa Fluor 555, and goat anti-guinea pig Alexa Fluor 647 were used. For pERK1/2 and p-mTOR experiments, goat anti-guinea pig Alexa Fluor 488, goat anti-mouse Alexa Fluor 568, and goat anti-rabbit Alexa Fluor 647 were used. After three more PBS washes, the glass bottoms containing stained neurons were detached from the dishes, mounted onto slides using DAPI Fluoromount-G mounting medium (SouthernBiotech), and sealed with nail polish.

Image acquisition and analysis. All images were acquired using a Plan-Apochromat 63×/1.40 oil objectives or a laser-scanning Fast AiryScan confocal microscope (LSM 880 FAS, Zeiss), with the exception of images in Figure 5*C–F* that were acquired on laser-scanning confocal microscope (LSM 880, Zeiss), using the ZEN Black acquisition software. Acquisition settings—including laser power, gain/offset, and pinhole size—were kept consistent across all experiments. During image acquisition, pyramidal neurons were identified by their characteristic teardrop-shaped somata and apical-like dendrites.

For each neuron, ∼15 stacked images (step size, 0.18 µm) were obtained to capture the apical dendrites and their branches and then subjected to maximum intensity projection using ZEN Black. To quantify synaptic protein colocalization and signal intensities, images were analyzed using the MetaMorph software (Molecular Devices).

A region of interest was manually drawn to include dendritic branches distal to the primary branch point of the apical-like dendrite. Signal intensity thresholds were set for each channel to exclude background noise, maintaining consistency across experimental groups. MetaMorph's granularity function was used to threshold puncta in each channel (puncta size, 0.5–5 µm). Binary images were generated to outline identified puncta, and colocalized puncta were determined using the Logical AND operation.

A synapse was defined as a punctum double-labeled with sGluA2 and VGluT1 (Figs. 1, 3*G*, 5, 6) or triple-labeled with GFP, sGluA2, and VGluT1 (Fig. 3*G*). Total puncta intensity for each channel at colocalized sites was then measured. For DHPG experiments, ImageJ was used to trace the soma area as regions of interest to quantify the mean intensity of pERK1/2 and phospho-mTOR signals.

Experimental design. Experimental conditions were run in parallel with the control condition on sister cultures from the same dissociation. The total puncta intensity measured in experimental conditions was normalized to the mean total puncta intensity of the control in sister cultures, unless otherwise specified.

Quantification and statistical analysis. All datasets were subjected to a normality test (Shapiro–Wilk test). For data with just a single comparison between two groups (i.e., control vs TTX), a Mann–Whitney *U* test was used. For experiments with two or more independent groups (i.e., WT UN vs P1311L UN, WT UN vs WT TTX, and P1311L UN vs P1311L TTX), a Kruskal–Wallis test with post hoc Dunn's multiple comparisons test was used. For experiments with two independent variables that may have an effect on a dependent variable (i.e., vehicle vs TTX, vehicle vs drug alone, drug alone vs drug + TTX), a two-way ANOVA followed by Tukey's post hoc correction was used for multiple comparisons. For plots of intensities for colocalized synaptic proteins (Figs. 1, 2, 4) which were not normally distributed, Spearman coefficients were used to determine the strength of correlation; the dotted lines on these figures represent the line that fits most of the data. In order to find the statistical line of best fit, the data were $\log_{10}$ transformed to achieve normality, and the degree of correlation was found by calculating Pearson's coefficients. For correlations of $\log_{10}$ transformed data, the *F* test was used to determine significance between the slopes of best-fit lines for control and TTX conditions. To compare correlation coefficients of the $\log_{10}$ transformed data, Fisher's *z* transformation was used to determine significant comparisons between control and TTX. Results were considered significant if $p < 0.05$. Significance symbols used in figures are defined as $*p < 0.05$; $**p < 0.01$; $***p < 0.001$; and n.s., not significant.

Data availability. All data generated in this study are included in the manuscript and available upon request.

Results

Shank3 is an essential mediator of synaptic scaling, but the signaling pathways downstream of Shank3 phosphorylation that translate a drop in neuronal firing into a homeostatic enhancement of synaptic AMPAR accumulation are largely unknown. Here we ask whether Shank3 and long-form Homer1 interactions, agonist-dependent Group I mGluR activity, and downstream group I mGluR canonical signaling pathways are necessary to enable synapses to undergo deprivation-induced synaptic upscaling.

Synaptic upscaling protocols enhance excitatory synaptic density and produce correlated changes in pre- and postsynaptic proteins

Previous work has shown that synaptic scaling is accompanied by changes in the abundance of many postsynaptic proteins, including Shank3 and Homer1 (Desch et al., 2021; Heavner et al., 2021; Wu et al., 2022; Yuan et al., 2023). In addition to modulating postsynaptic strength, some studies have also reported changes in the synapse number and presynaptic protein accumulation (Glebov et al., 2017; Dörrbaum et al., 2020), but these effects

are often smaller and more variable than changes in AMPAR accumulation. Here we compiled a large dataset (control $n = 120$; TTX treated $n = 104$ neurons) to determine the degree to which these pre- and postsynaptic changes are coupled. We induced synaptic upscaling by treating rat visual cortical cultures (used for all subsequent experiments, unless otherwise stated) with TTX for 24 h to suppress firing, transfected neurons at low efficiency with a fluorescent protein to allow us to carefully quantify synaptic contacts onto individual pyramidal neurons, then fixed and labeled them using antibodies directed against a surface epitope of the postsynaptic GluA2 subunit of the AMPAR (sGluA2) and the presynaptic glutamate transporter (VGluT1; Fig. 1*A*). The density of colocalized sGluA2 and VGluT1 puncta, which represent putative synaptic contacts, as well as the intensity of the fluorescent signals at these colocalized sites, was then quantified along apical-like pyramidal neuron dendrites. The postsynaptic accumulation of sGluA2 in TTX-treated neurons was enhanced compared with vehicle-treated neurons from sister cultures (Fig. 1*A*,*B*), as expected (Ibata et al., 2008; Tatavarty et al., 2013; Gainey et al., 2015; Wu et al., 2022). Furthermore, there was a small but significant increase in synaptic density (Fig. 1*C*) and a small but significant increase in the intensity of VGluT1 at presynaptic sites (Fig. 1*D*). To determine whether TTX produces correlated changes in pre- and postsynaptic markers at individual synapses, we plotted the intensity of VGluT1 versus sGluA2 for each synaptic contact for the control (Fig. 1*E*, $n = 4{,}398$) and TTX conditions (Fig. 1*F*, $n = 4{,}658$). Under both conditions there was a strong correlation (control $r^2 = 0.801$ vs TTX $r^2 = 0.785$); however, the line-of-best-fit slope of the relationship in the TTX condition is significantly steeper than control (Fig. 1*G*; control slope = 0.883 vs TTX slope = 0.927), consistent with a larger postsynaptic effect of synaptic scaling on sGluA2 accumulation than on VGlut1 levels (compare Fig. 1*B*,*D*). Thus, synaptic upscaling protocols induce coupled pre- and postsynaptic changes, as well as an increase in the synapse number.

Synaptic upscaling protocols enhance endogenous Shank3–Homer1 colocalization

Shank3 and Homer1 are known binding partners (Cheng et al., 2006), and both have been implicated in synaptic upscaling (Clifton et al., 2019; Tatavarty et al., 2020; Bockaert et al., 2021; Heavner et al., 2021; Wu et al., 2022). We therefore wished to explore how TTX treatment affects their colocalization at synaptic sites. To this end, we performed immunocytochemistry against Shank3 and Homer1b/c (using an antibody directed against a

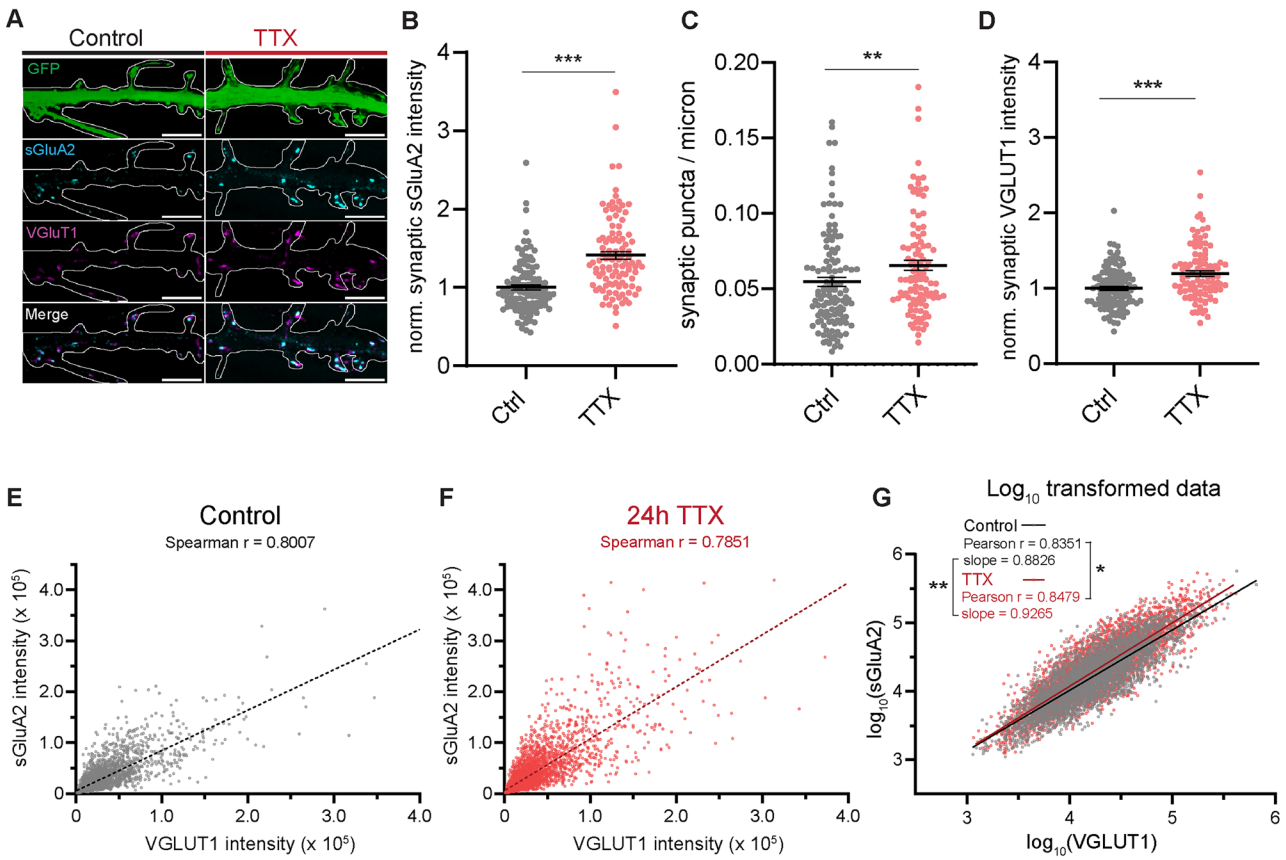

Figure 1. Synaptic scaling up protocols enhance excitatory synaptic density and produce correlated changes in pre- and postsynaptic proteins. ***A***, Representative images of sGluA2 and VGluT1 puncta in neuron expressing GFP and treated with DMSO vehicle (Ctrl) ± TTX (scale bar, 5 µm). ***B***, Quantification of synaptic sGluA2 intensity changes induced by scaling up protocol (number of neurons, control, $n = 120$; TTX, $n = 104$; Mann–Whitney *U* test: Ctrl vs TTX, $***p < 0.0001$). Solid horizontal black lines indicate mean, and error bars indicate SEM. ***C***, Quantification of putative synaptic puncta density changes induced by scaling up protocol (number of neurons, control, $n = 120$; TTX, $n = 104$; Mann–Whitney *U* test: Ctrl vs TTX, $**p = 0.0036$). ***D***, Quantification of synaptic VGLUT1 intensity changes induced by scaling up protocol (number of neurons, control, $n = 120$; TTX, $n = 104$; Mann–Whitney *U* test: Ctrl vs TTX, $***p < 0.0001$). ***E***, VGLUT1 intensity plotted against sGluA2 intensity for control condition. Linear best fit of non-normally distributed raw data shown in dotted line (number of puncta, UN, $n = 4{,}398$). ***F***, VGLUT1 intensity plotted against sGluA2 intensity for 24 h TTX treatment condition. Linear best fit of non-normally distributed raw data shown in dotted line (number of puncta, TTX, $n = 4{,}658$). ***G***, Log_{10} transformed data from ***E*** and ***F***. Line of best fit for each condition shown in solid lines (*F* test to determine lines are significantly different, line of best fit slope, $**p = 0.0003$). Fisher's *z* transformation was used to compare Pearson's correlation coefficients ($*p = 0.0457$).

sequence absent in Homer1a) and quantified the signal at colocalized sites within the apical dendrites of GFP-expressing neurons. The density of colocalized Shank3 and Homer1b/c puncta was approximately doubled after TTX treatment (Fig. 2*A*,*B*). Additionally, both Shank3 and Homer1b/c intensities at colocalized puncta were significantly increased in the TTX condition, to a similar degree (Fig. 2*C*,*D*). Finally, we examined the correlation between Shank3 and Homer1b/c intensity at individual puncta from control (Fig. 2*E*, $n = 1{,}511$) and TTX-treated neurons (Fig. 2*F*, $n = 2{,}228$). For both conditions, Shank3 and long-form Homer1 intensities were significantly correlated with each other, and the slopes of both relationships were similar and significantly different from zero (Fig. 2*E*,*F*). Interestingly, synaptic scaling was accompanied by a significant increase in both the slope of this relationship and the strength of correlation, suggesting that synaptic upscaling is accompanied by a greater and more tightly regulated association between Shank3 and long-form Homer1. Thus, while the short-form Homer1a has been linked to synaptic downscaling (Hu et al., 2010), these data implicate long-form Homer1 in synaptic upscaling.

Phosphomimetic Shank3 DD has reduced interaction with Homer1b/c but maintains its ability to localize to the synapse

Synaptic scaling reduces Shank3 phosphorylation at S1586/S1615, and overriding this dephosphorylation by overexpressing the phosphomimetic mutant Shank3 DD (Fig. 3*A*) blocks upscaling. In contrast, scaling up is preserved after overexpression of the phosphodeficient mutant Shank3 AA (Wu et al., 2022); while overexpression paradigms have potential limitations, we have established that neurons express normal synaptic levels of GluA2 and normal synaptic scaling after overexpression of WT Shank3 (Tatavarty et al., 2020; Wu et al., 2022). The ability of phosphomimetic Shank3 to block upscaling led us to wonder if the phosphorylation state of Shank3 might influence its ability to directly bind long-form Homer1. To test this, we cotransfected HEK-T cells with Homer1c plus one of several forms of GFP-tagged Shank3 (Fig. 3*A*): wild type (WT); phosphodeficient (AA); phosphomimetic (DD); or P1311L, a point mutant known to have significantly reduced binding to Homer1 proteins (Tu et al., 1999). Dynabeads bound to GFP antibody or GFP-trap magnetic beads/particles were used to pull down Shank3 protein from cell lysates, and Western blots were then performed to quantify the ratio of Homer1c to Shank3 (Fig. 3*B*). Shank3 WT and AA were able to pull down Homer1c with similar efficacy (AA was 88 ± 3.8% of WT) while the negative control P1311L had a greatly reduced efficacy (P1311L was 25.5 ± 6.5% of WT). Intriguingly, the phosphomimetic Shank3 DD mutant also had reduced efficacy in pulling down Homer1c (DD was 61.7 ± 4.8% of WT; Fig. 3*B*,*C*); there was no consistent difference in total amount of Shank3 pulled down across conditions (Fig. S1).

Next we assessed the ability of Shank3 DD and Shank3 P1311L to interfere with upscaling. Consistent with previous

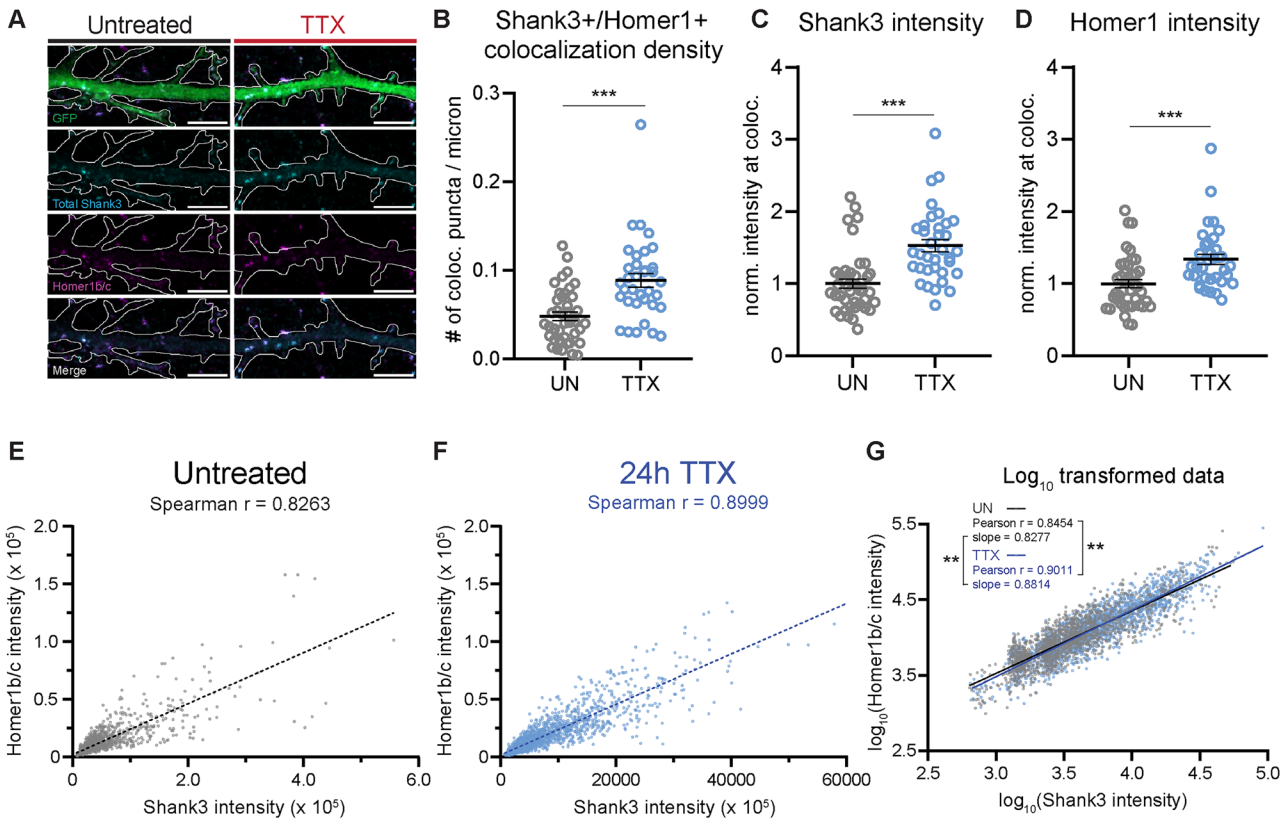

Figure 2. Synaptic scaling up protocols enhance endogenous Shank3–Homer1 colocalization. ***A***, Representative images of Shank3 and Homer1b/c puncta in dendrites from neurons expressing GFP (UN) ± TTX (scale bar, 5 µm). ***B***, Quantification of changes in Shank3+ Homer1b/c + puncta density induced by scaling up protocol (number of neurons, untreated, $n = 41$; TTX, $n = 35$; Mann–Whitney *U* test: UN vs TTX, $***p < 0.0001$). ***C***, Quantification of synaptic Shank3 intensity changes induced by scaling up protocol (number of neurons, untreated, $n = 41$; TTX, $n = 35$; Mann–Whitney *U* test: UN vs TTX, $***p < 0.0001$). ***D***, Quantification of synaptic Homer1b/c intensity changes induced by scaling up protocol (number of neurons, untreated, $n = 41$; TTX, $n = 35$; Mann–Whitney *U* test: UN vs TTX, $***p = 0.0002$). ***E***, Shank3 intensity plotted against Homer1 intensity for untreated condition. Linear best fit of non-normally distributed raw data shown in dotted line (number of puncta, UN, $n = 1{,}511$). ***F***, Shank3 intensity plotted against Homer1 intensity for 24 h TTX treatment condition. Linear best fit of non-normally distributed raw data shown in dotted line (number of puncta, TTX, $n = 2{,}228$). ***G***, Log_{10} transformed data from ***E*** and ***F***. Line of best fit for each condition shown in solid lines (*F* test to determine lines are significantly different, line of best fit slope, $**p = 0.0006$). Fisher's *z* transformation was used to compare Pearson's correlation coefficients ($***p < 0.0001$).

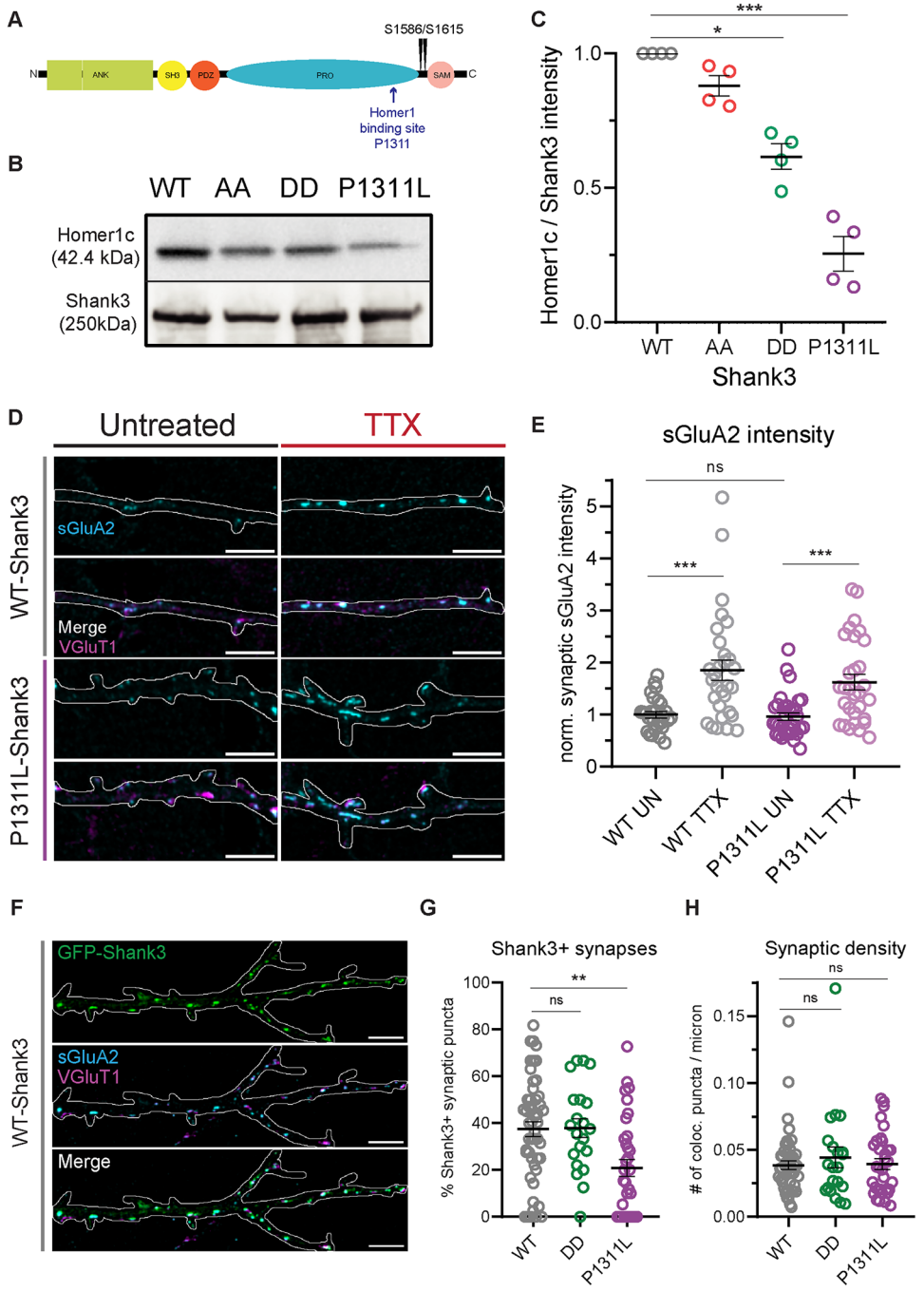

Figure 3. Phosphomimetic Shank3 DD has reduced interaction with Homer1b/c but maintains its ability to localize to the synapse. ***A***, Schematic of full-length Shank3 (Shank3 WT) with various domains, Shank3 phosphorylation sites of interest, and P1311L point mutation location labeled. ***B***, Representative Western blot image of Homer1c and Shank3 bands corresponding to Shank3 pulldowns of lysate from HEK cells overexpressing various Shank3 constructs. ***C***, Quantification of Western blot from Shank3 pulldowns by plotting Homer1c intensity value divided by corresponding Shank3 band intensity (4 biological replicates with each normalized to Homer1c band intensity divided by WT Shank3 band intensity value, Kruskal–Wallis test with post hoc Dunn's multiple-comparison test, WT vs AA, ns $p = 0.6939$; WT vs DD, $*p = 0.05$; WT vs P1311L, $**p = 0.001$). ***D***, Representative images of GFP-tagged Shank3, VGluT1, and sGluA2 puncta from WT and P1311L Shank3 overexpressing neurons. ***E***, Quantification of synaptic sGluA2 intensity changes induced by scaling up protocol in WT and P1311L Shank3 overexpressing neurons (UN) ± TTX (number of neurons, WT UN, $n = 28$; WT TTX, $n = 30$; P1311L UN, $n = 33$; P1311L TTX, $n = 30$; Kruskal–Wallis test with post hoc Dunn's multiple-comparison test, WT UN vs P1311L UN, ns $p > 0.9999$; WT UN vs WT TTX, $***p = 0.0005$; P1311L UN vs P1311L TTX, ns $***p = 0.0005$). ***F***, Representative images of GFP-tagged Shank3, VGluT1, and sGluA2 puncta from WT, DD, and P1311L Shank3 overexpressing neurons. ***G***, Quantification of percentage Shank3 + synapses out of the total number of synapses represented by sGluA2 and VGluT1 colocalizations in WT, DD, and P1311L Shank3 overexpressing neurons (number of neurons, WT, $n = 50$; DD, $n = 21$; P1311L, $n = 33$; Kruskal–Wallis test with post hoc Dunn's multiple-comparison test, WT vs DD, ns $p > 0.9999$; WT vs P1311L, $**p = 0.0017$). ***H***, Quantification of synaptic density in WT, DD, and P1311L Shank3 overexpressing neurons (number of neurons, WT, $n = 50$; DD, $n = 21$; P1311L, $n = 33$; Kruskal–Wallis test with post hoc Dunn's multiple-comparison test, WT vs DD, ns $p > 0.9999$; WT vs P1311L, ns $p > 0.9999$).

work (Wu et al., 2022), neurons expressing Shank3 DD were unable to express upscaling; in contrast, neurons overexpressing the point mutant Shank3 P1311L exhibited normal synaptic scaling (Fig. 3*D*,*E*). We next examined the synaptic localization of both forms of mutant Shank3 relative to WT, by examining the fraction of putative synaptic puncta (defined as sites of colocalization of sGluA2 and VGluT1) that contain tagged Shank3. Interestingly, while Shank3 DD localized to synaptic sites to

the same degree as WT Shank3, Shank3 P1311L had greatly reduced synaptic localization (Fig. S2; Fig. 3*F*,*G*). This reduced synaptic localization may explain why Shank3 P1311L is not able to prevent synaptic scaling up, as this effect presumably relies on displacing endogenous Shank3 from synapses (Fig. 3*E*). Finally, we verified that overexpressing these Shank3 mutants did not affect the density of puncta colocalizing sGluA2 and VGluT1; indeed we found no significant differences in the density of putative synapses between neurons overexpressing Shank3 WT, DD, and P1311L (Fig. 3*H*).

Synaptic upscaling protocols do not alter Shank3–Homer1 colocalization or produce correlated changes between these proteins in the presence of phosphomimetic Shank3 DD

If Shank3 phosphorylation at S1586/S1615 disrupts the association between Shank3 and long-form Homer1 at synapses, we would expect that TTX treatment would no longer enhance Homer1 accumulation in the presence of Shank3 DD. To test this, we transfected sister cultures at low efficiency with GFP-tagged Shank3 DD and quantified the degree of colocalization of total Shank3 (endogenous and overexpressed) and endogenous Homer1b/c. In the presence of Shank3 DD, TTX treatment did not significantly increase the density of colocalized puncta (Fig. 4*A*,*B*). Furthermore, the intensity of Shank3 and Homer1b/c signals at colocalized sites was not altered by TTX treatment (Fig. 4*C*,*D*).

Next, we examined the correlation between Shank3 and Homer1b/c intensity at individual puncta from neurons expressing Shank3 DD, without (Fig. 4*E*, $n = 1{,}842$) or with (Fig. 4*F*, $n = 1{,}105$) TTX treatment. In the untreated condition, Shank3 and long-form Homer1 intensities were significantly correlated with each other (Fig. 4*E*). Strikingly, while this correlation normally increases after TTX treatment (Fig. 2*E*,*F*), in the presence of Shank3 DD, there was instead a robust decrease in correlation after TTX treatment (Fig. 4*E*,*F*, from $r^2 = 0.881$ to $r^2 = 0.779$), as well as a significant decrease in slope (Fig. 4*G*, from 0.322 to 0.247). Thus, Shank3 DD (but not WT Shank3 overexpression) disrupts the ability of activity blockade to enhance the association between Shank3 and long-form Homer1, consistent with the ability of Shank3 DD (but not WT) to block upscaling

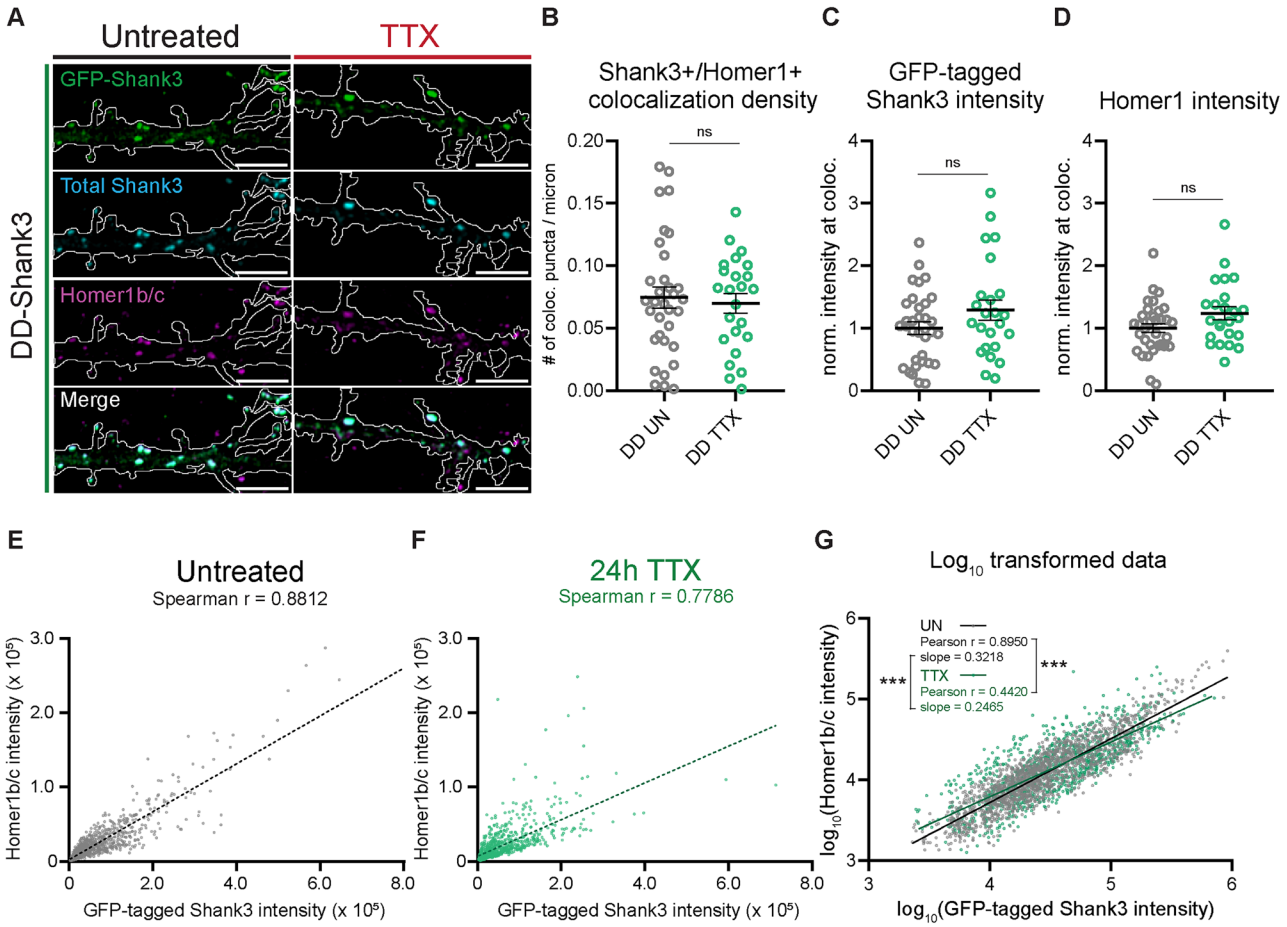

Figure 4. Synaptic scaling up protocols do not alter Shank3–Homer1 colocalization nor produce correlated changes between these proteins in the presence of phosphomimetic Shank3 DD. ***A***, Representative images of GFP-tagged Shank3 and Homer1b/c puncta in dendrites from Shank3 DD overexpressing neurons (UN) ± TTX (scale bar, 5 µm). ***B***, Quantification of changes in Shank3 + Homer1b/c + puncta number induced by scaling up protocol from Shank3 DD overexpressing neurons (number of neurons, DD untreated (UN), $n = 33$; DD TTX, $n = 24$; unpaired *t* test with Welch's correction, DD UN vs DD TTX, ns $p = 0.6876$). ***C***, Quantification of GFP-tagged Shank3 DD intensity changes induced by scaling up protocol from Shank3 DD overexpressing neurons (number of neurons, DD UN, $n = 33$; DD TTX, $n = 24$; unpaired *t* test with Welch's correction, DD UN vs DD TTX, ns $p = 0.1342$). ***D***, Quantification of synaptic Homer1b/c intensity changes induced by scaling up protocol from Shank3 DD overexpressing neurons (number of neurons, DD UN, $n = 33$; DD TTX, $n = 24$; unpaired *t* test with Welch's correction, DD UN vs DD TTX, ns $p = 0.0664$). ***E***, GFP-tagged Shank3 DD intensity plotted against Homer1 intensity for untreated condition. Linear best fit of non-normally distributed raw data shown in dotted line (number of puncta, UN, $n = 1{,}842$). ***F***, GFP-tagged Shank3 DD intensity plotted against Homer1 intensity for 24 h TTX treatment condition. Linear best fit of non-normally distributed raw data shown in dotted line (number of puncta, TTX, $n = 1{,}105$). ***G***, Log_{10} transformed data from ***E*** and ***F***. Line of best fit for each condition shown in solid lines (*F* test to determine lines are significantly different, line of best fit slope, $***p < 0.0001$). Fisher's *z* transformation was used to compare Pearson's correlation coefficients ($***p < 0.0001$).

(Tatavarty et al., 2020). To ensure that this effect does not rely on the presence of high levels of endogenous Shank3, we repeated this experiment after knockdown of endogenous Shank3 as described (Tatavarty et al., 2020; Wu et al., 2022; note our Shank3 DD and WT constructs are insensitive to the shRNA) and obtained similar results (Fig. S3). Together, these data suggest that Shank3 DD may block synaptic upscaling by preventing the enhanced association between Shank3 and long-form Homer1.

Agonist-dependent Group I mGluR signaling is necessary for scaling up and enhanced mGlur5 activity rescues synaptic scaling up in the presence of phosphomimetic Shank3 DD

Long-form Homer1 links Shank proteins, including Shank3, to Group I mGluRs to modulate signaling (Wang et al., 2016b). We thus wondered whether Shank3 DD might block scaling up by preventing activation of Group I mGluRs. Group I mGluRs are present at the perisynapse and have both agonist-dependent and agonist-independent activity (Ango et al., 2001; Bockaert et al., 2021; Mango and Ledonne, 2023). It is known that Group I mGluR noncompetitive inhibitors, specifically those thought to target agonist-independent signaling, can abolish homeostatic synaptic downscaling (Hu et al., 2010), but the role of mGluR signaling in upscaling has not been assessed. Therefore, we began by testing the ability of the noncompetitive inhibitors BAY 36-7620 (mGluR1) and MTEP (mGluR5) to block synaptic upscaling. Cotreatment of cultures with TTX and these noncompetitive inhibitors for 24 h resulted in an increase in synaptic AMPAR accumulation of similar magnitude to that produced by TTX alone (Fig. 5*A*,*B*, MTEP + BAY vs MTEP + BAY TTX; Table 1), suggesting that agonist-independent activity of Group I mGluRs is not necessary for synaptic upscaling to occur.

Agonist-independent activity is important for downscaling (Hu et al., 2010) and can result from binding to short-form Homer1a (Ango et al., 2001; Clifton et al., 2019). We next wondered whether, in contrast, competitive inhibition (likely targeting agonist-dependent activity) of the Group I mGluRs might be the critical signal needed for synaptic upscaling. To test this, we cotreated cultures for 24 h with TTX and *S*-4-CPG, a specific competitive inhibitor of Group I mGluRs. We found that competitive inhibition led to a complete loss of synaptic upscaling (Fig. 5*A*,*B*, S4CPG vs S4CPG TTX; Table 1). Thus, upscaling and downscaling are differentially affected by competitive and noncompetitive (respectively) Group I mGluR inhibition.

We showed previously that Shank3 DD traffics correctly to synaptic sites and blocks upscaling (Wu et al., 2022); if this effect is mediated through a reduction in Group I mGluR signaling, then enhancing this signaling should rescue scaling up in the presence of Shank3 DD. Because the two Group I mGluRs, mGluR1 and mGluR5, have some distinct and some overlapping functions and actions, we decided to selectively target mGluR5 with CDPPB, a positive allosteric modulator of mGluR5. CDDPB binds to a site on mGluR5 that is distinct from the ligand binding site, to enhance the response to binding of the endogenous ligand, glutamate. We first ensured that CDPPB does not affect upscaling in the presence of WT Shank3 overexpression; in neurons expressing WT Shank3, synaptic sGluA2 intensity was unaffected by CDPPB at the baseline, and TTX induced the normal increase in the presence of CDPPB (Fig. 5*C*,*D*). When we overexpressed Shank3 DD and treated neurons with TTX, synaptic upscaling was absent (Fig. 5*E*,*F*), as expected (Wu et al., 2022). However, cotreatment of Shank3 DD overexpressing neurons with CDPPB and TTX induced robust synaptic upscaling (Fig. 5*E*,*F*); CDPPB treatment alone in Shank3 DD overexpressing neurons did not affect baseline synaptic sGluA2 intensity (Fig. S4). Thus, enhancement of mGluR5 function is sufficient to rescue synaptic scaling up; furthermore, this demonstrates that mGluR5 signaling is downstream of Shank3 phosphorylation in the signaling pathways mediating synaptic scaling up.

Competitive and noncompetitive inhibition of Group I mGluRs target different downstream pathways

MGluR signaling is complex, and in neocortical neurons, it is not completely understood which downstream pathways are affected by competitive versus noncompetitive inhibition (Ronesi et al., 2012; Bockaert et al., 2021). Phosphorylation of ERK1/2 (Mao et al., 2005) and mTOR (Page et al., 2006) are known to be downstream of Group I mGluR activation, so we probed for a differential effect of competitive and noncompetitive mGluR inhibitors on this phosphorylation. Neurons were pretreated with either competitive or noncompetitive inhibitors for 45 min, the Group I mGluR agonist DHPG was added for 15 min, and the cultures were then fixed and stained against pERK1/2 or p-mTOR and the somatic signal quantified and compared with untreated neurons. Noncompetitive inhibition with MTEP + BAY blocked the increase in p-mTOR and reduced but did not fully prevent the increase in pERK1/2, while the competitive inhibitor S4CPG had no impact on either pathway (Fig. 6*A*–*C*). Thus, in these neocortical cultures, competitive and noncompetitive Group I mGluR inhibition affect distinct downstream signaling pathways.

Canonical Group I mGluR downstream signaling pathways are necessary for synaptic scaling up

We next wanted to investigate which pathway(s) downstream of Group I mGluRs is necessary for homeostatic synaptic upscaling. The canonical pathway(s) downstream of group I mGluRs is driven by Gq/G11-dependent activation of PLC that leads to PKC activation and also to mobilization of intracellular calcium from internal stores (Conn and Pin, 1997; Hermans and Challiss, 2001; Mango and Ledonne, 2023). Given that S4CPG blocks upscaling but has no effect on several noncanonical signaling pathways in our neocortical cultures (Fig. 6), we targeted the canonical pathway (Fig. 7*A*), focusing on branches of the signaling cascade where selective inhibitors are available, to determine their necessity for synaptic upscaling.

To target PLC, we used the selective PLC inhibitor, aminosteroid U73122 (Kamato et al., 2015; Neacsu et al., 2020). We found that TTX was unable to increase synaptic AMPAR accumulation in the presence of U73122 (Fig. 7*B*,*C*, U73122 vs U73122 + TTX; Table 2), indicating that synaptic scaling is impaired under these conditions. One target of PLC activation is Ca^{2+} release from intracellular stores, which is modulated by the sarcoplasmic–endoplasmic reticulum Ca^{2+} ATPase (SERCA-ATPase; Masu et al., 1991; Abe et al., 1992; Putney and Tomita, 2012). We used the selective SERCA-ATPase inhibitor CPA, which has been shown to deplete internal calcium stores in hippocampal neurons (Eder and Bading, 2007), to target this pathway. Because it takes time to deplete intracellular stores of calcium, the SERCA-ATPase inhibitor CPA was added to the culture media 6 h before TTX, and cultures were fixed and labeled 24 h after TTX addition. Interestingly, there was a significant increase in the sGluA2 synaptic intensity for the CPA + TTX condition compared with the CPA only condition

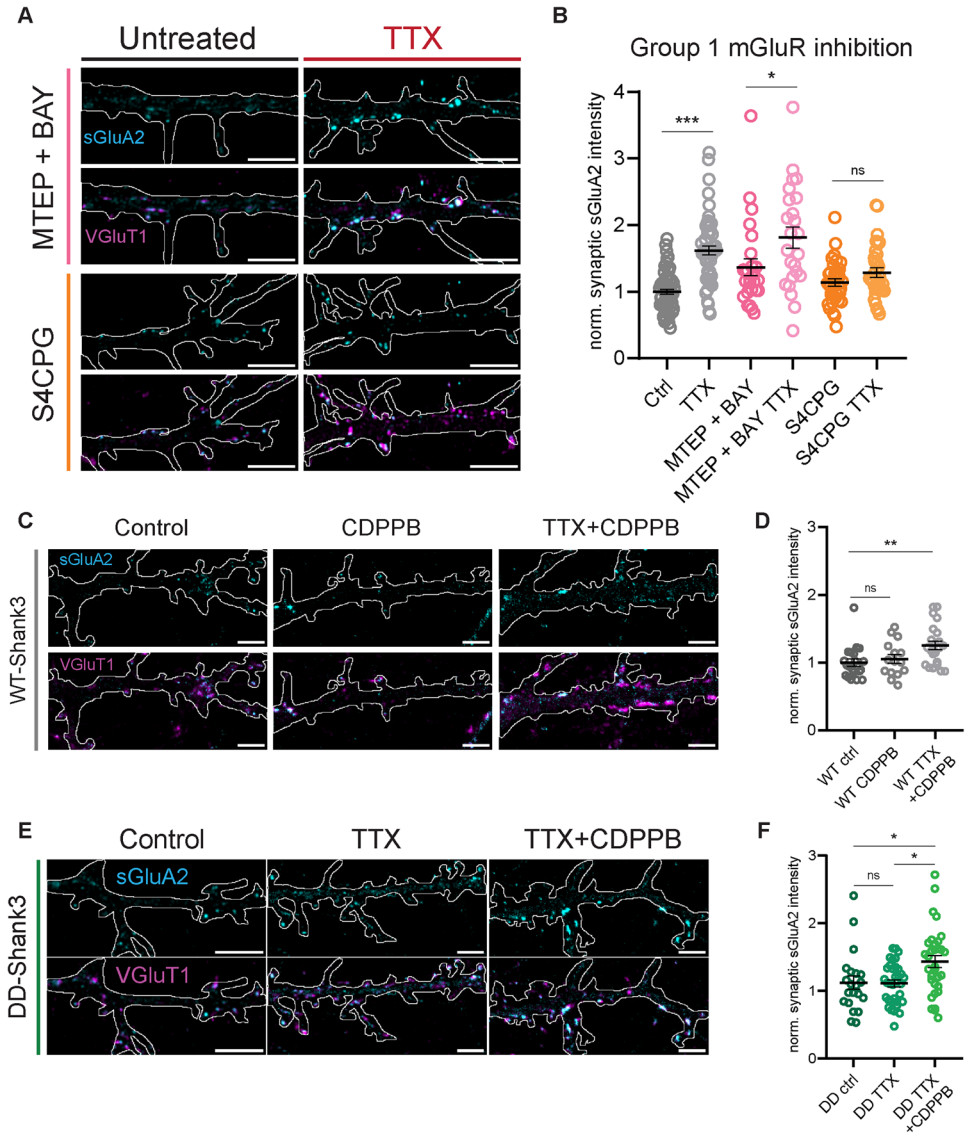

Figure 5. Agonist-dependent group I mGluR signaling is necessary for scaling up and enhanced mGluR5 activity rescues synaptic scaling up in the presence of phosphomimetic Shank3 DD. ***A***, Representative images of synaptic puncta colocalized with sGluA2 and VGLUT1 in neuron dendrites treated with DMSO or 100 mM NaOH vehicle (Ctrl) ± TTX, MTEP + BAY ± TTX, and *S*-4-CPG ± TTX (scale bar, 5 µm). ***B***, Quantification of synaptic sGluA2 intensity changes induced by scaling up protocol (Dataset 1, number of neurons, control, $n = 29$; TTX, $n = 24$; MTEP + BAY, $n = 26$; MTEP + BAY TTX, $n = 24$; two-way ANOVA with post hoc Tukey's multiple-comparison test, Ctrl vs TTX, $^{**}p = 0.0030$; Ctrl vs MTEP + BAY, ns $p = 0.0711$; MTEP + BAY vs MTEP + BAY TTX, $^{*}p = 0.0236$; Dataset 2, number of neurons, control, $n = 32$; TTX, $n = 30$; *S*-4-CPG, $n = 36$; *S*-4-CPG TTX, $n = 33$; two-way ANOVA with post hoc Tukey's multiple-comparison test, Ctrl vs TTX, $^{***}p < 0.0001$; Ctrl vs *S*-4-CPG, ns $p = 0.5223$; *S*-4-CPG vs *S*-4-CPG TTX, ns $p = 0.4529$). ***C***, Representative images of synaptic puncta colocalized with sGluA2 and VGLUT1 in dendrites of WT Shank3 overexpressing neurons treated with DMSO vehicle (ctrl) ± CDPPB (CDPPB) ± TTX (CDPPB + TTX; scale bar, 5 µm). ***D***, Quantification of putative synaptic puncta changes induced by scaling up protocol (number of neurons, WT ctrl, $n = 21$; WT CDPPB, $n = 15$; WT CDPPB + TTX, $n = 22$; Kruskal–Wallis test with post hoc Dunn's multiple-comparison test, WT ctrl vs WT CDPPB, ns $p = 0.9817$; WT ctrl vs WT CDPPB + TTX, $^{**}p = 0.0058$). ***E***, Representative images of synaptic puncta colocalized with sGluA2 and VGLUT1 in dendrites of DD Shank3 overexpressing neurons treated with DMSO vehicle (ctrl) ± TTX (TTX) ± CDPPB (TTX + CDPPB; scale bar, 5 µm). ***F***, Quantification of putative synaptic puncta changes induced by scaling up protocol (number of neurons, DD ctrl, $n = 15$; DD TTX, $n = 31$; DD TTX + CDPPB, $n = 38$; Kruskal–Wallis test with post hoc Dunn's multiple-comparison test, DD ctrl vs DD TTX, ns $p > 0.9999$; DD ctrl vs DD CDPPB + TTX, $^{**}p = 0.0033$; DD TTX vs DD TTX + CDPPB, $^{*}p = 0.0115$).

Table 1. Two-way ANOVA for MTEP + BAY and *S*-4-CPG experiments

ANOVA table	SS (Type III)	Degrees of freedom	Mean squares	$F_{(DFn,\ DFd)}$	*p* value
Interaction (MTEP + BAY)	0.05378	1	0.05378	$F_{(1,\ 99)} = 0.1793$	$p = 0.6729$
Effect of TTX on Veh	6.273	1	6.273	$F_{(1,\ 99)} = 20.92$	$p < 0.0001$
Effect of TTX on MTEP + BAY	2.611	1	2.611	$F_{(1,\ 99)} = 8.708$	$p = 0.0040$
Residual (MTEP + BAY)	29.69	99	0.2999		
Interaction (*S*-4-CPG)	2.324	1	2.324	$F_{(1,\ 127)} = 13.41$	$p = 0.0004$
Effect of TTX on Veh	5.625	1	5.625	$F_{(1,\ 127)} = 32.47$	$p < 0.0001$
Effect of TTX on *S*-4-CPG	0.5401	1	0.5401	$F_{(1,\ 127)} = 3.117$	$p = 0.0799$
Residual (*S*-4-CPG)	22.00	127	0.1732		

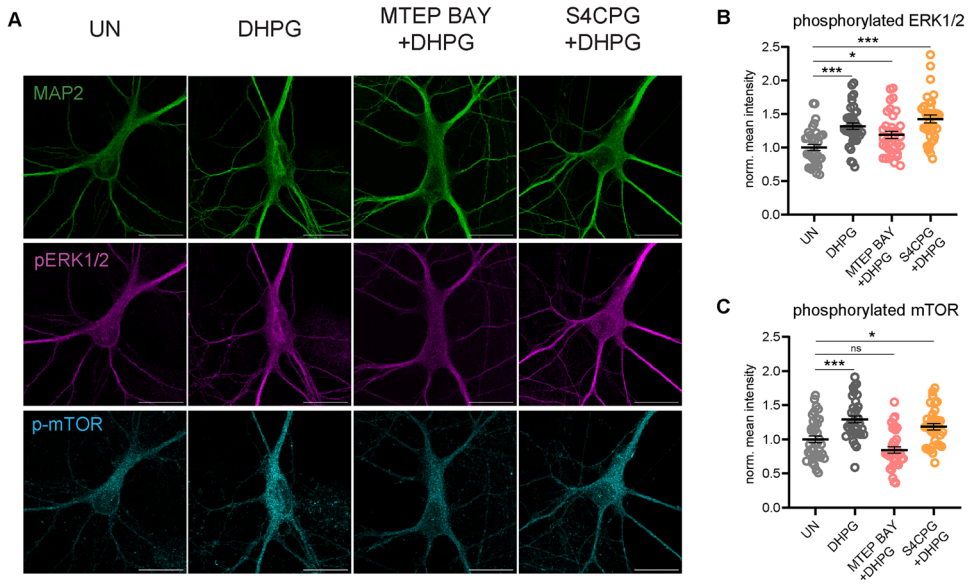

Figure 6. Noncompetitive and competitive inhibition may function through distinct mechanisms downstream of Group I mGluRs. ***A***, Representative images of neurons in untreated (UN), DHPG, MTEP BAY + DHPG, and S4CPG + DHPG conditions labeled with MAP2 and their corresponding pERK1/2 and phospo-mTOR signal (scale bar, 20 µm). ***B***, Quantification of phosphorylated ERK1/2 intensity from soma (number of neurons, UN, $n = 38$; DHPG, $n = 36$; MTEP BAY + DHPG, $n = 36$; S4CPG + DHPG, $n = 34$; Kruskal–Wallis test with post hoc Dunn's multiple-comparison test, UN vs DHPG, $***p < 0.0001$; UN vs MTEP BAY, +DHPG, $*p = 0.0419$; UN vs S4CPG, $***p < 0.0001$). ***C***, Quantification of phosphorylated mTOR intensity from soma (number of neurons, UN, $n = 38$; DHPG, $n = 36$; MTEP BAY + DHPG, $n = 36$; S4CPG + DHPG, $n = 34$' Kruskal–Wallis test with post hoc Dunn's multiple-comparison test, UN vs DHPG, $***p = 0.0008$; UN vs MTEP BAY + DHPG, ns $p = 0.1364$; UN vs S4CPG, $*p = 0.0379$).

(Fig. 7*B*,*C*; Table 2), suggesting that intact internal calcium stores are not essential for synaptic upscaling.

Finally, we examined the other major target of the Gq/G11-mediated Group I mGluR signaling, PKC. To test for a role of PKC, we used the broad-spectrum PKC inhibitor, GO6983, to target all isoforms of PKC (Gschwendt et al., 1996; Zheng et al., 2000). In the presence of GO6983, TTX was unable to increase synaptic sGluA2 relative to inhibitor GO6983 alone (Fig. 7*B*,*C*; Table 2). These findings show that multiple branches of the Group I mGluR canonical pathway signaling cascade are necessary for the induction of synaptic scaling up.

Taken together, our data suggest that synaptic upscaling is enabled when Shank3 dephosphorylation regulates binding with Homer1b/c, which biases Group I mGluR activity toward agonist-dependent signaling through the canonical pathway (Fig. 7*D*).

Discussion

While synaptic scaling has been studied extensively in a wide variety of contexts (Desai et al., 2002; Wierenga et al., 2005; Goel and Lee, 2007; Ibata et al., 2008; Steinmetz and Turrigiano, 2010; Sun and Turrigiano, 2011; Tatavarty et al., 2013; Gainey et al., 2015; Steinmetz et al., 2016; Wu et al., 2022), the pathways downstream of Shank3 dephosphorylation are unknown. Here, we utilize genetic and pharmacological manipulations to show that Group I mGluR activity, and key components of its downstream canonical signaling pathways are required for upscaling. Importantly, the Shank3 phosphorylation state influences binding interactions with long-form Homer1, suggesting that the impact of Shank3 phosphorylation state on mGluR activity is achieved through the modulation of Shank3/long-form Homer1 interactions. Together, our findings support a unified model in which the same molecular players known to be crucial for synaptic downscaling during activity enhancement—Shank3, Homer1 isoforms, and group I mGluRs—are reconfigured by activity deprivation to enable the distinct and complementary signaling required for synaptic upscaling.

Previous work has shown that synaptic scaling down is blocked by noncompetitive inhibition of Group I mGluRs, suggesting that it depends on agonist-independent activity (Hu et al., 2010; Diering et al., 2017). In this model of downscaling, high network activity leads to an increase in the immediate early gene Homer1a; Homer1a then functions as a dominant negative to prevent the crosslinking of synaptic proteins, including Shank3 and Group I mGluRs. By displacing long-form Homer1, Homer1a is able to bind group I mGluRs to evoke mGluR constitutive, or agonist-independent, activity. This constitutive mGluR activity is required for synaptic downscaling, through a signaling cascade that involves phosphorylation of extracellular signal–regulated kinase 1/2 (ERK1/2; Hu et al., 2010; Diering et al., 2017).

Here, we define a complementary signaling pathway during synaptic upscaling that uses activity-dependent changes in the phosphoproteome to rearrange the same signaling elements from a configuration that enables downscaling into one that instead enables upscaling. We find that prolonged activity deprivation enhances the association between Shank3 and long-form Homer1, in a manner that depends on the Shank3 phosphorylation state. Moreover, we find that competitive, rather than noncompetitive, inhibition of Group I mGluRs prevents the expression of synaptic upscaling; furthermore, we find that these inhibitors have distinct effects on downstream signaling pathways. Together with previous work showing that downscaling protocols initiate constitutive mGluR signaling that is blocked by noncompetitive antagonists (Bockaert et al., 2021), our data suggest that up- and downscaling protocols result in several reciprocal changes that influence Shank3/Homer1/mGluR associations: first, they alter the Shank3 phosphorylation state and Homer1 short-form abundance to bias Shank3/Homer associations toward Homer1 long-form (upscaling) or short-form (downscaling), and second, as a consequence of these altered

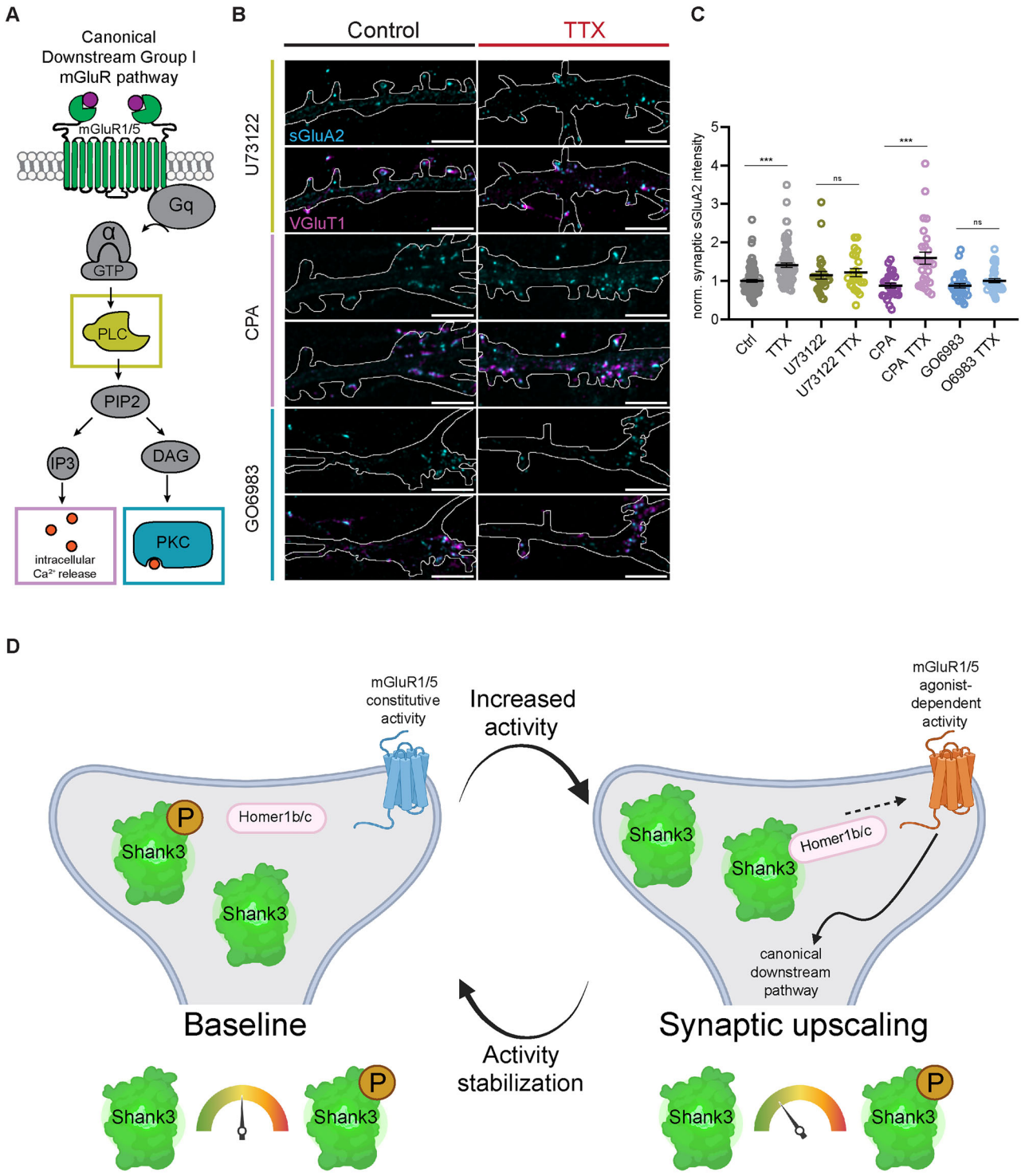

Figure 7. Canonical Group I mGluR downstream signaling pathways are necessary for synaptic scaling up. ***A***, Diagram depicting key elements of canonical pathway downstream of Group I mGluRs highlighting targeted proteins and processes. ***B***, Representative images of synaptic puncta colocalized with sGluA2 and VGLUT1 in neuron dendrites treated with DMSO vehicle (Ctrl) ± TTX and U73122 ± TTX, CPA ± TTX, and GO6983 ± TTX (scale bar, 5 µm). ***C***, Quantification of synaptic sGluA2 intensity changes induced by scaling up protocol (Dataset 1, number of neurons, control, $n = 26$; TTX, $n = 22$; U73122, $n = 27$; U73122 TTX, $n = 23$; two-way ANOVA with post hoc Tukey's multiple-comparison test, Ctrl vs TTX, $^{**}p = 0.0093$; Ctrl vs U73122, ns $p = 0.6709$; U73122 vs U73122 TTX, ns $p = 0.9592$; Dataset 2, number of neurons, control, $n = 35$; TTX, $n = 29$; CPA, $n = 26$; CPA TTX, $n = 27$; two-way ANOVA with post hoc Tukey's multiple-comparison test, Ctrl vs TTX, $^{*}p = 0.0253$; Ctrl vs CPA ns $p = 0.8416$; CPA vs CPA TTX, $^{***}p < 0.0001$; Dataset 3, number of neurons, control; $n = 30$; TTX, $n = 25$; GO6983, $n = 31$; GO6983 TTX, $n = 33$; two-way ANOVA with post hoc Tukey's multiple-comparison test, Ctrl vs TTX $^{***}p = 0.0001$; Ctrl vs GO6983, ns $p = 0.3848$; GO6983 vs GO6983 TTX, ns $p = 0.3265$). ***D***, Proposed model illustrating how synaptic upscaling (right side) during activity blockade leads to predominance of dephosphorylated Shank3 to allow for increased association with Homer1b/c. Synaptic upscaling also requires a shift in Group I mGluRs to agonist-dependent activity and downstream activation of the canonical signaling pathway (Created with Biorender.com).

associations, mGluR5 signaling is switched from agonist-dependent (upscaling) to agonist-independent (downscaling) signaling modes.

In addition to the Shank3–Homer1 interaction, associations between other members of this proposed pathway may be actively modulated during synaptic upscaling. For instance,

Table 2. Two-way ANOVA for U73122, CPA, and G06983 experiments

ANOVA table	SS (Type III)	Degrees of freedom	Mean squares	$F_{(DFn,\ DFd)}$	*p* value
Interaction (U73122)	0.8607	1	0.8607	$F_{(1,\ 93)} = 3.754$	$p = 0.0557$
Effect of TTX on Veh	1.597	1	1.597	$F_{(1,\ 93)} = 6.968$	$p = 0.0097$
Effect of TTX on U73122	0.03907	1	0.03907	$F_{(1,\ 93)} = 0.1704$	$p = 0.6807$
Residual (U73122)	21.32	93	0.2293		
Interaction (CPA)	1.145	1	1.145	$F_{(1,\ 117)} = 3.466$	$p = 0.0651$
Effect of TTX on Veh	8.027	1	8.027	$F_{(1,\ 117)} = 24.30$	$p < 0.0001$
Effect of TTX on CPA	0.1629	1	0.1629	$F_{(1,117)} = 0.4932$	$p = 0.4839$
Residual (CPA)	38.64	117	0.3303		
Interaction (G06983)	0.4209	1	0.4209	$F_{(1,\ 115)} = 4.427$	$p = 0.0376$
Effect of TTX on Veh	1.854	1	1.854	$F_{(1,\ 115)} = 19.50$	$p < 0.0001$
Effect of TTX on G06983	1.776	1	1.776	$F_{(1,\ 115)} = 18.68$	$p < 0.0001$
Residual (G06983)	10.93	115	0.09507		

phosphorylation of the EVH1 domain of Homer1 (Guo et al., 2015) and the C-terminal domain of mGluR5 (Park et al., 2013) have been shown to influence Homer1–mGluR5 binding and thus remain to be investigated in the context of synaptic upscaling. Furthermore, the interaction between Homer1a and mGluR5 is necessary for the association between mGluR5 and NMDAR (Moutin et al., 2012), while disrupting Homer1–mGluR5 interactions influences the AMPA:NMDA ratio and decreases ERK and mTOR activation (Moutin et al., 2021). In future work, it will be interesting to determine whether dynamic modulation of the Homer1–mGluR5 binding interaction also plays an important role in synaptic upscaling.

Group I mGluR activation can initiate signaling through a number of downstream effectors. Because Homer1a displaces Group I mGluRs from the major signaling effectors inositol 1,4,5-triphosphate and PKC (IP3R/PKC; Brakeman et al., 1997), this likely biases signaling toward other pathways (Diering et al., 2017). Binding of long-form Homer and Group I mGluRs results in a switch from constitutive to agonist-dependent mGluR activity (Fagni et al., 2003), consistent with our observation that upscaling is blocked by competitive mGluR antagonists and requires downstream PLC and PKC signaling. Interestingly, mGluR-dependent long–term depression is dependent on the presence of Shank3 (Lee et al., 2019), and mGluR-dependent forms of LTP require intracellular calcium release regulated by SERCA-ATPase, IP3-receptors, and ryanodine receptors (Holbro et al., 2009; Lüscher and Huber, 2010; Wang et al., 2016a; Chami and Checler, 2020). Our finding that intact internal calcium stores are not necessary for synaptic upscaling further suggests that distinct forms of synaptic plasticity utilize different downstream mGluR signaling pathways.

We find that synaptic upscaling is blocked by the competitive antagonist S4CPG, but not by the noncompetitive antagonists MTEP + BAY. S4CPG prevents the DHPG-induced production of diacylglycerol (Herrero et al., 1998) and also blocks Group I mGluR agonist-induced intracellular calcium oscillations (Flint et al., 1999). These studies suggest that S4CPG acts through the canonical downstream mGluR1/5 pathway, in agreement with our findings that other major downstream pathways, involving pERK1/2 and phospho-mTOR activity, are not affected by S4CPG treatment. However, given the complexity of agonist dependent and independent (constitutive) mGluR signaling (Niswender and Conn, 2010; Ribeiro et al., 2017; Bockaert et al., 2021; Abd-Elrahman and Ferguson, 2022), delineating the mechanism of action of competitive versus noncompetitive antagonists in up- and downscaling may be complex. For instance, BAY and MTEP also target glutamate-induced increase in IP formation (Carroll et al., 2001) and IP hydrolysis (Lea et al., 2005), respectively, suggesting that in some cell types, these noncompetitive antagonists act in part through the canonical pathway, in addition to targeting mTOR and ERK signaling.

There are a host of molecular players that have been implicated in synaptic scaling up (Pozo and Goda, 2010; Wen and Turrigiano, 2024), suggesting that Shank3/Homer1/mGluR5 signaling likely works in concert with additional signaling and trafficking pathways to enhance synaptic AMPAR accumulation. Since mGluR signaling is able to regulate transcription, one possibility is that this pathway could be important for transcriptional changes necessary for synaptic upscaling (Ibata et al., 2008; Steinmetz et al., 2016; Schaukowitch et al., 2017). Another interesting possibility is that Shank3/Homer1/mGluR complexes might influence Shank3 binding to GRIP1 (Sheng and Kim, 2000) to enable GRIP1 to capture AMPARs at the PSD (Gainey et al., 2015; Tan et al., 2015). An important point is that mGluR5 signaling is not sufficient to induce scaling up; rather, this pathway, like upstream Shank3 phosphorylation, serves to gate the direction of homeostatic compensation.

Our data suggest that TTX-induced synaptic scaling up requires agonist-dependent mGluR signaling. This raises the interesting question of what drives agonist-dependent activity of Group I mGluRs in the presence of TTX, which blocks spike-mediated glutamate release. One likely possibility is that spike-independent, spontaneous vesicular release of glutamate is sufficient to activate mGluR signaling during activity blockade. Given the predominantly perisynaptic localization of Group I mGluRs (Scheefhals and MacGillavry, 2018; Scheefhals et al., 2023) and reports that spontaneous release happens in areas that encompass synaptic and perisynaptic sites (Tang et al., 2016; Farsi et al., 2021), spontaneous release may be well placed to activate these receptors.

Taken together, our work suggests a model in which activity-dependent changes in Shank3 phosphorylation modulate Shank3 interactions with long-form Homer1, leading to a switch from constitutive to agonist-dependent activity of Group I mGluRs to enable synaptic scaling up. This supports the possibility that autism spectrum disorder (ASD) phenotypes arising from *Shank3* loss (Moessner et al., 2007; Zhou et al., 2016; Bey et al., 2018) may be caused in part through disrupted signaling through Group I mGluRs, as has been suggested for other ASD-associated genes such as FMR1 (Huber et al., 2002; Nakamoto et al., 2007; Iliff et al., 2013).

References

Abd-Elrahman KS, Ferguson SSG (2022) Noncanonical metabotropic glutamate receptor 5 signaling in Alzheimer's disease. Annu Rev Pharmacol Toxicol 62:235–254.

Abe T, Sugihara H, Nawa H, Shigemoto R, Mizuno N, Nakanishi S (1992) Molecular characterization of a novel metabotropic glutamate receptor mGluR5 coupled to inositol phosphate/Ca2+ signal transduction. J Biol Chem 267:13361–13368.

Ango F, Prézeau L, Muller T, Tu JC, Xiao B, Worley PF, Pin JP, Bockaert J, Fagni L (2001) Agonist-independent activation of metabotropic glutamate receptors by the intracellular protein Homer. Nature 411:962–965.

Bey AL, et al. (2018) Brain region-specific disruption of Shank3 in mice reveals a dissociation for cortical and striatal circuits in autism-related behaviors. Transl Psychiatry 8:94.

Bockaert J, Perroy J, Ango F (2021) The complex formed by group I metabotropic glutamate receptor (mGluR) and Homer1a plays a central role in metaplasticity and homeostatic synaptic scaling. J Neurosci 41:5567–5578.

Brakeman PR, Lanahan AA, O'Brien R, Roche K, Barnes CA, Huganir RL, Worley PF (1997) Homer: a protein that selectively binds metabotropic glutamate receptors. Nature 386:284–288.

Carroll FY, et al. (2001) BAY36-7620: a potent non-competitive mGlu1 receptor antagonist with inverse agonist activity. Mol Pharmacol 59: 965–973.

Chami M, Checler F (2020) Alterations of the endoplasmic reticulum (ER) calcium signaling molecular components in Alzheimer's disease. Cells 9:2577.

Cheng D, et al. (2006) Relative and absolute quantification of postsynaptic density proteome isolated from rat forebrain and cerebellum. Mol Cell Proteomics 5:1158–1170.

Clifton NE, Trent S, Thomas KL, Hall J (2019) Regulation and function of activity-dependent Homer in synaptic plasticity. Complex Psychiatry 5: 147–161.

Conn PJ, Pin J-P (1997) Pharmacology and functions of metabotropic glutamate receptors. Annu Rev Pharmacol Toxicol 37:205–237.

Desai NS, Cudmore RH, Nelson SB, Turrigiano GG (2002) Critical periods for experience-dependent synaptic scaling in visual cortex. Nat Neurosci 5: 783–789.

Desch K, Langer JD, Schuman EM (2021) Dynamic bi-directional phosphorylation events associated with the reciprocal regulation of synapses during homeostatic up- and down-scaling. Cell Rep 36:109583.

Diering GH, Nirujogi RS, Roth RH, Worley PF, Pandey A, Huganir RL (2017) Homer1a drives homeostatic scaling-down of excitatory synapses during sleep. Science 355:511–515.

Dörrbaum AR, Alvarez-Castelao B, Nassim-Assir B, Langer JD, Schuman EM (2020) Proteome dynamics during homeostatic scaling in cultured neurons. Elife 9:e52939.

Eder A, Bading H (2007) Calcium signals can freely cross the nuclear envelope in hippocampal neurons: somatic calcium increases generate nuclear calcium transients. BMC Neurosci 8:57.

Fagni L, Ango F, Prezeau L, Worley PF, Pin J-P, Bockaert J (2003) Control of constitutive activity of metabotropic glutamate receptors by Homer proteins. Int Congr Ser 1249:245–251.

Farsi Z, Walde M, Klementowicz AE, Paraskevopoulou F, Woehler A (2021) Single synapse glutamate imaging reveals multiple levels of release mode regulation in mammalian synapses. iScience 24:101909.

Flint AC, Dammerman RS, Kriegstein AR (1999) Endogenous activation of metabotropic glutamate receptors in neocortical development causes neuronal calcium oscillations. Proc Natl Acad Sci U S A 96:12144–12149.

Gainey MA, Hurvitz-Wolff JR, Lambo ME, Turrigiano GG (2009) Synaptic scaling requires the GluR2 subunit of the AMPA receptor. J Neurosci 29:6479–6489.

Gainey MA, Tatavarty V, Nahmani M, Lin H, Turrigiano GG (2015) Activity-dependent synaptic GRIP1 accumulation drives synaptic scaling up in response to action potential blockade. Proc Natl Acad Sci U S A 112: E3590–E3599.

Glebov OO, Jackson RE, Winterflood CM, Owen DM, Barker EA, Doherty P, Ewers H, Burrone J (2017) Nanoscale structural plasticity of the active zone matrix modulates presynaptic function. Cell Rep 18:2715–2728.

Goel A, Lee H-K (2007) Persistence of experience-induced homeostatic synaptic plasticity through adulthood in superficial layers of mouse visual cortex. J Neurosci 27:6692–6700.

Goold CP, Nicoll RA (2010) Single-cell optogenetic excitation drives homeostatic synaptic depression. Neuron 68:512–528.

Grabrucker AM, Schmeisser MJ, Schoen M, Boeckers TM (2011) Postsynaptic ProSAP/Shank scaffolds in the cross-hair of synaptopathies. Trends Cell Biol 21:594–603.

Gschwendt M, Dieterich S, Rennecke J, Kittstein W, Mueller H-J, Johannes F-J (1996) Inhibition of protein kinase C μ by various inhibitors. Inhibition from protein kinase c isoenzymes. FEBS Lett 392:77–80.

Guo W, Ceolin L, Collins KA, Perroy J, Huber KM (2015) Elevated CaMKIIα and hyperphosphorylation of Homer mediate circuit dysfunction in a fragile X syndrome mouse model. Cell Rep 13:2297–2311.

Hayashi MK, Tang C, Verpelli C, Narayanan R, Stearns MH, Xu R-M, Li H, Sala C, Hayashi Y (2009) The postsynaptic density proteins Homer and Shank form a polymeric network structure. Cell 137:159–171.

Heavner WE, Lautz JD, Speed HE, Gniffke EP, Immendorf KB, Welsh JP, Baertsch NA, Smith SEP (2021) Remodeling of the Homer–Shank interactome mediates homeostatic plasticity. Sci Signal 14:eabd7325.

Hermans E, Challiss RAJ (2001) Structural, signalling and regulatory properties of the group I metabotropic glutamate receptors: prototypic family C G-protein-coupled receptors. Biochem J 359:465–484.

Herrero I, Miras-Portugal MT, Sánchez-Prieto J (1998) Functional switch from facilitation to inhibition in the control of glutamate release by metabotropic glutamate receptors. J Biol Chem 273:1951–1958.

Holbro N, Grunditz Å, Oertner TG (2009) Differential distribution of endoplasmic reticulum controls metabotropic signaling and plasticity at hippocampal synapses. Proc Natl Acad Sci U S A 106:15055–15060.

Hu J-H, et al. (2010) Homeostatic scaling requires group I mGluR activation mediated by Homer1a. Neuron 68:1128–1142.

Huber KM, Gallagher SM, Warren ST, Bear MF (2002) Altered synaptic plasticity in a mouse model of fragile X mental retardation. Proc Natl Acad Sci U S A 99:7746–7750.

Ibata K, Sun Q, Turrigiano GG (2008) Rapid synaptic scaling induced by changes in postsynaptic firing. Neuron 57:819–826.

Iliff AJ, Renoux AJ, Krans A, Usdin K, Sutton MA, Todd PK (2013) Impaired activity-dependent FMRP translation and enhanced mGluR-dependent LTD in fragile X premutation mice. Hum Mol Genet 22:1180–1192.

Jiang Y, Ehlers MD (2013) Modeling autism by SHANK gene mutations in mice. Neuron 78:8–27.

Kamato D, Thach L, Bernard R, Chan V, Zheng W, Kaur H, Brimble M, Osman N, Little PJ (2015) Structure, function, pharmacology, and therapeutic potential of the G protein, $G\alpha_{q,11}$. Front Cardiovasc Med 2:1–11.

Lautz JD, Brown EA, Williams VanSchoiack AA, Smith SEP (2018) Synaptic activity induces input-specific rearrangements in a targeted synaptic protein interaction network. J Neurochem 146:540–559.

Lea PM, Movsesyan VA, Faden AI (2005) Neuroprotective activity of the mGluR5 antagonists MPEP and MTEP against acute excitotoxicity differs and does not reflect actions at mGluR5 receptors. Br J Pharmacol 145: 527–534.

Lee K, Vyas Y, Garner CC, Montgomery JM (2019) Autism-associated *Shank3* mutations alter mGluR expression and mGluR-dependent but not NMDA receptor-dependent long-term depression. Synapse 73:e22097.

Louros SR, Caldeira GL, Carvalho AL (2018) Stargazin dephosphorylation mediates homeostatic synaptic downscaling of excitatory synapses. Front Mol Neurosci 11:328.

Lüscher C, Huber KM (2010) Group 1 mGluR-dependent synaptic long-term depression: mechanisms and implications for circuitry and disease. Neuron 65:445–459.

Mango D, Ledonne A (2023) Updates on the physiopathology of group I metabotropic glutamate receptors (mGluRI)-dependent long-term depression. Cells 12:1588.

Mao L, Yang L, Tang Q, Samdani S, Zhang G, Wang JQ (2005) The scaffold protein Homer1b/c links metabotropic glutamate receptor 5 to extracellular signal-regulated protein kinase cascades in neurons. J Neurosci 25: 2741–2752.

Masu M, Tanabe Y, Tsuchida K, Shigemoto R, Nakanishi S (1991) Sequence and expression of a metabotropic glutamate receptor. Nature 349:760–765.

Moessner R, et al. (2007) Contribution of SHANK3 mutations to autism spectrum disorder. Am J Hum Genet 81:1289–1297.

Moutin E, Raynaud F, Roger J, Pellegrino E, Homburger V, Bertaso F, Ollendorff V, Bockaert J, Fagni L, Perroy J (2012) Dynamic remodeling of scaffold interactions in dendritic spines controls synaptic excitability. J Cell Biol 198:251–263.

Moutin E, et al. (2021) Restoring glutamate receptosome dynamics at synapses rescues autism-like deficits in Shank3-deficient mice. Mol Psychiatry 26:7596–7609.

Naisbitt S, Kim E, Tu JC, Xiao B, Sala C, Valtschanoff J, Weinberg RJ, Worley PF, Sheng M (1999) Shank, a novel family of postsynaptic density proteins

that binds to the NMDA receptor/PSD-95/GKAP complex and cortactin. Neuron 23:569–582.
Nakamoto M, Nalavadi V, Epstein MP, Narayanan U, Bassell GJ, Warren ST (2007) Fragile X mental retardation protein deficiency leads to excessive mGluR5-dependent internalization of AMPA receptors. Proc Natl Acad Sci U S A 104:15537–15542.
Neacsu C, Sauer SK, Reeh PW, Babes A (2020) The phospholipase C inhibitor U73122 is a potent agonist of the polymodal transient receptor potential ankyrin type 1 (TRPA1) receptor channel. Naunyn Schmiedebergs Arch Pharmacol 393:177–189.
Niswender CM, Conn PJ (2010) Metabotropic glutamate receptors: physiology, pharmacology, and disease. Annu Rev Pharmacol Toxicol 50:295–322.
O'Brien RJ, Kamboj S, Ehlers MD, Rosen KR, Fischbach GD, Huganir RL (1998) Activity-dependent modulation of synaptic AMPA receptor accumulation. Neuron 21:1067–1078.
Page G, Khidir FAL, Pain S, Barrier L, Fauconneau B, Guillard O, Piriou A, Hugon J (2006) Group I metabotropic glutamate receptors activate the p70S6 kinase via both mammalian target of rapamycin (mTOR) and extracellular signal-regulated kinase (ERK 1/2) signaling pathways in rat striatal and hippocampal synaptoneurosomes. Neurochem Int 49:413–421.
Park JM, et al. (2013) A prolyl-isomerase mediates dopamine-dependent plasticity and cocaine motor sensitization. Cell 154:637–650.
Pozo K, Goda Y (2010) Unraveling mechanisms of homeostatic synaptic plasticity. Neuron 66:337–351.
Pratt KG, Watt AJ, Griffith LC, Nelson SB, Turrigiano GG (2003) Activity-dependent remodeling of presynaptic inputs by postsynaptic expression of activated CaMKII. Neuron 39:269–281.
Putney JW, Tomita T (2012) Phospholipase C signaling and calcium influx. Adv Biol Regul 52:152–164.
Ribeiro FM, Vieira LB, Pires RGW, Olmo RP, Ferguson SSG (2017) Metabotropic glutamate receptors and neurodegenerative diseases. Pharmacol Res 115:179–191.
Ronesi JA, Collins KA, Hays SA, Tsai N-P, Guo W, Birnbaum SG, Hu J-H, Worley PF, Gibson JR, Huber KM (2012) Disrupted Homer scaffolds mediate abnormal mGluR5 function in a mouse model of fragile X syndrome. Nat Neurosci 15:431–440.
Schaukowitch K, Reese AL, Kim S-K, Kilaru G, Joo J-Y, Kavalali ET, Kim T-K (2017) An intrinsic transcriptional program underlying synaptic scaling during activity suppression. Cell Rep 18:1512–1526.
Scheefhals N, Westra M, MacGillavry HD (2023) Mglur5 is transiently confined in perisynaptic nanodomains to shape synaptic function. Nat Commun 14:244.
Scheefhals N, MacGillavry HD (2018) Functional organization of postsynaptic glutamate receptors. Mol Cell Neurosci 91:82–94.
Sheng M, Kim E (2000) The Shank family of scaffold proteins. J Cell Sci 113: 1851–1856.
Steinmetz CC, Turrigiano GG (2010) Tumor necrosis factor-α signaling maintains the ability of cortical synapses to express synaptic scaling. J Neurosci 30:14685–14690.
Steinmetz CC, et al. (2016) Upregulation of μ3A drives homeostatic plasticity by rerouting AMPAR into the recycling endosomal pathway. Cell Rep 16: 2711–2722.
Stillman M, Lautz JD, Johnson RS, MacCoss MJ, Smith SEP (2022) Activity dependent dissociation of the Homer1 interactome. Sci Rep 12:3207.
Sun Q, Turrigiano GG (2011) PSD-95 and PSD-93 play critical but distinct roles in synaptic scaling up and down. J Neurosci 31:6800–6808.
Tan HL, Queenan BN, Huganir RL (2015) GRIP1 is required for homeostatic regulation of AMPAR trafficking. Proc Natl Acad Sci U S A 112:10026–10031.
Tang A-H, Chen H, Li TP, Metzbower SR, MacGillavry HD, Blanpied TA (2016) A trans-synaptic nanocolumn aligns neurotransmitter release to receptors. Nature 536:210–214.
Tatavarty V, Sun Q, Turrigiano GG (2013) How to scale down postsynaptic strength. J Neurosci 33:13179–13189.
Tatavarty V, Torrado Pacheco A, Groves Kuhnle C, Lin H, Koundinya P, Miska NJ, Hengen KB, Wagner FF, Van Hooser SD, Turrigiano GG (2020) Autism-associated Shank3 is essential for homeostatic compensation in rodent V1. Neuron 106:769–777.e4.
Tu JC, et al. (1999) Coupling of mGluR/Homer and PSD-95 complexes by the Shank family of postsynaptic density proteins. Neuron 23:583–592.
Turrigiano GG (2008) The self-tuning neuron: synaptic scaling of excitatory synapses. Cell 135:422–435.
Turrigiano GG, Nelson SB (2004) Homeostatic plasticity in the developing nervous system. Nat Rev Neurosci 5:97–107.
Turrigiano GG, Leslie KR, Desai NS, Rutherford LC, Nelson SB (1998) Activity-dependent scaling of quantal amplitude in neocortical neurons. Nature 391:892–896.
Venkatesan S, Subramaniam S, Rajeev P, Chopra Y, Jose M, Nair D (2020) Differential scaling of synaptic molecules within functional zones of an excitatory synapse during homeostatic plasticity. eNeuro 7: ENEURO.0407-19.2020.
Verpelli C, et al. (2011) Importance of Shank3 protein in regulating metabotropic glutamate receptor 5 (mGluR5) expression and signaling at synapses. J Biol Chem 286:34839–34850.
Wang H, et al. (2016a) Metabotropic glutamate receptors induce a form of LTP controlled by translation and arc signaling in the hippocampus. J Neurosci 36:1723–1729.
Wang X, et al. (2016b) Altered mGluR5-Homer scaffolds and corticostriatal connectivity in a Shank3 complete knockout model of autism. Nat Commun 7:11459.
Wen W, Turrigiano GG (2024) Keeping your brain in balance: homeostatic regulation of network function. Annu Rev Neurosci 47:41–61.
Wierenga CJ, Ibata K, Turrigiano GG (2005) Postsynaptic expression of homeostatic plasticity at neocortical synapses. J Neurosci 25:2895–2905.
Wu C-H, et al. (2022) A bidirectional switch in the Shank3 phosphorylation state biases synapses toward up- or downscaling. Elife 11:e74277.
Yuan X, et al. (2023) A human in vitro neuronal model for studying homeostatic plasticity at the network level. Stem Cell Reports 18:2222–2239.
Zheng W-H, Kar S, Quirion R (2000) Stimulation of protein kinase C modulates insulin-like growth factor-1-induced Akt activation in PC12 cells. J Biol Chem 275:13377–13385.
Zhou Y, et al. (2016) Mice with Shank3 mutations associated with ASD and schizophrenia display both shared and distinct defects. Neuron 89:147–162.